Pharm Res (2016) 33:603–614
DOI 10.1007/s11095-015-1813-0

RESEARCH PAPER

Biodistribution and Toxicity of X-Ray Iodinated Contrast Agent in Nano-emulsions in Function of Their Size

Mohamed F. Attia[1,2,3] • Nicolas Anton[1,2] • Roman Akasov[1,2,4] • Manuela Chiper[1,2] • Elena Markvicheva[4] • Thierry F. Vandamme[1,2]

Received: 7 September 2015 / Accepted: 21 October 2015 / Published online: 28 October 2015

ABSTRACT

Purpose This study aimed to investigate the impact of the size of X-ray iodinated contrast agent in nano-emulsions, on their toxicity and fate *in vivo*.

Methods A new compound, triiodobenzoate cholecalciferol, was synthetized, formulated as nano-emulsions, and followed after i.v. administration in mice by X-ray imaging (micro computed tomography). Physicochemical characterization and process optimization allowed identifying a good compromise between X-ray contrasting properties, monodispersity and stability. This also allowed selecting two formulations with different sizes, hydrodynamic diameters of 55 and 100 nm, but exactly the same composition. *In vitro* experiments were performed on two cell lines, namely hepatocytes (BNL-CL2) and macrophages (RAW264.7).

Results Cell viability studies, cell uptake observations by confocal microscopy, and uptake quantification by fluorimetry, disclosed clear differences between two formulations, as well as between two types of cell lines. After i.v. injection of the two iodinated nano-emulsions in mice, CT scans provided the quantification of the pharmacokinetics and biodistributions. We finally showed that the size in the nano-emulsions has not a real impact on the pharmacokinetics and biodistributions, but has a strong influence on their toxicity, corroborating the *in vitro* results.

Conclusions This study shows that the size of the nanocarrier significantly matters, likely due to highly different interactions with cells and tissues.

KEY WORDS cholecalciferol · contrast agent · emulsion size · micro-CT · nano-emulsion

ABBREVIATIONS

$CDCl_3$	Deuterated chloroform
CT	Computed tomography
DCC	N,N′-dicyclohexylcarbodiimide
DLS	Dynamic light scattering
DMAP	4-dimethylaminopyridine
DMEM	Dulbecco's modified Eagle medium
DMSO	Dimethyl sulfoxide
EPR	Enhanced permeation and retention
FBS	Fetal bovine serum
HBSS	Hank's balanced salt solution
microCT	Micro computed tomography
MRI	Magnetic resonance imaging
MTT	3-(4,5 dimethylthiazol-2-yl)-2,5-diphenyltetrazolium bromide
NPs	Nanoparticles
OR	Oil ratio
PBS	Phosphate buffered saline
PDI	Polydispersity index
PEG	Polyethyleneglycol
PET	Positron emission tomography
RES	Reticuloendothelial system
SOR	Surfactant / (surfactant + oil) weight ratio

Electronic supplementary material The online version of this article (doi:10.1007/s11095-015-1813-0) contains supplementary material, which is available to authorized users.

✉ Nicolas Anton
nanton@unistra.fr

[1] University of Strasbourg, Faculty of Pharmacy, 74 route du Rhin 67401 Illkirch Cedex, France

[2] CNRS UMR 7199, Laboratoire de Conception et Application de Molécules Bioactives, équipe de Pharmacie Biogalénique, University of Strasbourg, route du Rhin No. 74, F-67401 Illkirch Cedex, France

[3] National Research Center, P.O. 12622, Cairo, Egypt

[4] Shemyakin-Ovchinnikov Institute of Bioorganic Chemistry, Russian Academy of Sciences, Miklukho-Maklaya Str., 16/10 117997 Moscow, Russia

SOWR	(surfactant + oil) / (surfactant + oil + water) weight ratio
SPECT	Single photon emission computed tomography
TIBA	2,3,5-Triiodobenzoic acid
TMS	Tetramethylsilane

INTRODUCTION

Advanced diagnosis is becoming a prime and essential step for ideal treatment by means of detecting pathogens and showing the specific locations of unhealthy cells. In this context, non-invasive and minimally invasive *in vivo* imaging techniques constitute a powerful arsenal for clinical diagnostics, and are currently seeing an unprecedented development. Several imaging modalities such as X-ray computed tomography (X-Ray CT), magnetic resonance imaging (MRI), positron emission tomography (PET) and single photon emission computed tomography (SPECT) or combination among two or more different modalities (multi-modals) are utilized for obtaining high resolution and potential visibility of internal bodily structures. They are generally complementary with their specific balance between advantage and drawbacks. Herein, we are focusing on X-ray imaging, that can be considered as an interesting compromise between cost, with a good spatial resolution, and without managing radioactive wastes as it is the case for nuclear imaging. On the other hand, extents X-ray imaging is very limited without using contrast agents, can only reveals bones structures and in any case soft tissues and biological compartment like blood vessels, tissues, organs. Contrast agents must be administrated along with the X-ray scanning, in order to improve contrast enhancement. Relevance and potency of "ideal" contrast agent are still largely dependent on their *in vivo* behavior, biodistribution and pharmacokinetics. More precisely, in this work, our interest concerns the development of contrast agents for preclinical X-ray CT (microCT), using scanners designed for small laboratory animals, and in this case the clinical contrast agents are not applicable since they undergo a fast blood clearance by kidneys avoiding animal imaging, and *a fortiori* targeted imaging. Strictly speaking, renal cut off size is 5.5 nm. However, when we refer to a suspension of nanoparticles (NPs) the whole distribution should be higher to this threshold to avoid renal clearance. This is generally why we can consider that increasing the size of the contrast agent in the form of NPs bigger than 50 nm (diameter) prevents the early renal clearance. The ideal NP contrast agent must fulfill a number of stringent requirements, briefly enumerated in the following: *(i)* the contrast agent should be easily dispersible and highly stable in a variety of local *in vivo* environments; *(ii)* the contrast agent should exhibit limited nonspecific binding and be resistant to reticuloendothelial system (RES) uptake (1,2), generally done with a specific surface coating with polyethyleneglycol (PEG) (3–5). As a result, the blood circulation time is prolonged, increasing the chance for the nanoparticles to bind with specific targets. *(iii)* Specifically for preclinical microCT imaging, the contrast agent must be big enough (average diameter> 50 nm) to avoid the fast renal clearance as discussed above (6). *(iv)* Depending of the application, a control of the surface composition can be necessary to promote the particle targeting to specific sites (7,8); this can be achieved through passive targeting, e.g., according to enhanced permeation and retention effect (EPR), or mediated by ligand decoration of the surface (e.g., antigen, cell, tissue). *(v)* A very important point that oriented the nature of the particle is the loading rate of a radiopaque material. Indeed, X-ray imaging modality is related to a very high concentration of contrasting materials administrated along with a nontoxicity (9,10). *(vi)* The facile synthesis resulting in high yield of purified compounds make them promising candidates and thereby translated successfully into clinical advances. Ideally, those kinds of materials will be efficient for long-term quantitative imaging at low doses and be safely cleared from the body after the imaging is completed. To gather all these points, iodine-based nano-emulsions, have recently been developed showing huge stability, high biocompatibility and great potential in medical applications, such as image-guided surgery, advanced diagnosis (e.g., to recognize tumor regions), personalized medicine or theragnostics.

We previously reported (11) the formulation of non-toxic iodinated nano-emulsions based on natural compounds like vitamin E, triglycerides, monoglycerides. The choice of the system is driven by the hypothesis that molecules that naturally occur in living organisms would exhibit a better compatibility and non-toxicity. In the present study, we propose to evaluate a new molecule that has never been explored as a contrast agent, namely cholecalciferol (or vitamin D_3) covalently modified with a triiodobenzene functionality. Cholecalciferol is an essential lipid soluble vitamin, one of the important ingredients in a human daily diet. It is photosynthesized in the human body from 7-dehydrocholesterol when exposed to U.V. wavelengths of light (12,13), and it is metabolized in the liver and kidney (14–17). Inspired by its biocompatibility, biodegradability and structural similarity with cholesterol, which is an important component of cellular membranes, and due to its poor water-solubility and low bioavailability, cholecalciferol is often encapsulated within lipid-based delivery systems for improving its bioaccessibility.

Herein, we focus on iodinated cholecalciferol as a non-toxic model contrast agent, in order to follow the expected blood pool imaging and then its passive accumulation in liver. In previous reports, we showed that the nature of the iodinated oil constituting the droplet core has a drastic influence on the biodistribution of the contrast agent (11). In the present study, we propose to keep constant the formulation composition and to focus only on the effect of the size of the

nanoparticulate contrast agent on its *in vivo* behavior and distribution. In fact, in literature, many studies showed that physicochemical factors can affect biodistribution and toxicity of nanoparticles (18–20). It is well approved that the particle size and surface charge can affect the efficiency and pathway of cellular uptake for liposomes (21), quantum dots (22), polymeric NPs (23,24), gold NPs (25), and silica NPs (26) by influencing the adhesion of the particles and their interaction with cells (27). However, this question has never been pointed out for nano-emulsions, and, in the case of iodinated nano-emulsions, can potentially serve in controlling the properties of the contrast agents. Above the smallest sizes that induce the renal clearance (i.e., below 50 nm), a legitimate question concerns the potential impact of the nanoparticle size regarding the immune system and organs cell uptake, and thus its influence on the biodistribution. In this study, we synthetized a new contrast agent, triiodobenzoate cholecalciferol that was formulated as PEGylated nano-emulsions through spontaneous emulsification with two different and representative sizes (average diameters) of 55 and 100 nm. These formulations were studied *in vitro* and their imaging properties, pharmacokinetics and biodistribution were followed *in vivo* by micro-CT after i.v. administration in mice.

EXPERIMENTAL SECTION

Materials

Cholecalciferol (Vitamin D_3), 2,3,5-Triiodobenzoic acid (TIBA), 4-dimethylaminopyridine (DMAP), N,N′-dicyclohexylcarbodiimide (DCC), dichloromethane, ethyl acetate, cyclohexane, sodium hydrogen carbonate, sodium sulfate anhydrous, sodium chloride, Hoechst 33258, calcein AM, deuterated chloroform ($CDCl_3$), dimethyl sulfoxide (DMSO) and 3-(4,5 dimethylthiazol-2-yl)-2,5-diphenyltetrazolium bromide (MTT) solutions were purchased from Sigma Aldrich (St. Louis, MO), Labrafac® WL1349 (Gattefossé S.A., Saint-Priest, France) is a mixture of capric and caprylic acid triglycerides. Non-ionic surfactant (Kolliphor ELP®) from BASF (Ludwigshafen, Germany) is a parenteral grade non-ionic surfactant made by reacting ethylene oxide with castor seed oil at an ethylene oxide to oil molar ratio of 35 (28). The product mainly consists of a PEG chain (35 ethylene glycol units) grafted onto a molecule of castor oil, Phosphate buffered saline (PBS), Dulbecco's modified Eagle medium (DMEM), Penicillin/Streptomycin solution (10.000 Units Penicillin/ml and 10 mg Streptomycin/ml) and fetal bovine serum (FBS) were obtained from PAN Biotech (Aidenbatch, Germany), and 0.22 μm syringe filters were purchased from Fisher (Germany).

Methods

Synthesis and Characterization of Cholecalciferoyl 2,3,5-Triiodobenzoate

The incorporation of iodine into the oily molecule was performed via a simple esterification reaction. Thus 2,3,5-triiodobenzoic acid (5 g, 0.01 mol), 4-dimethylaminopyridine (0.183 g, 0.0015 mol) and N,N′-dicyclohexylcarbodiimide (2.26 g, 0.011 mol) were sequentially added to a solution of cholecalciferol (3.08 g, 0.008 mol) in dicholoromethane (250 mL) at room temperature. The reaction mixture was kept under stirring overnight at room temperature, and then dicyclohexylurea and other precipitates were removed by filtration. The organic phase was further washed twice with aqueous $NaHCO_3$ (5%), once with saturated NaCl solution and dried over anhydrous Na_2SO_4. The solvent was removed in vacuum and the obtained precipitate was then purified by gradient elution chromatography on silica gel using cyclohexane and ethyl acetate as eluents. The reaction yield was 43% and the final product obtained as a yellow needle-like crystals revealed a high iodine content (approximately 44% of the molecular weight). The synthesis scheme of cholecalciferoyl 2,3,5-triiodobenzoate is shown in Fig. 1 (top).

^{1}H-NMR Analysis

^{1}H-NMR spectra were recorded with a Bruker Top Spin 3.0 operating at 400 MHz using deuterated chloroform ($CDCl_3$) as a solvent. Chemical shifts (δ) were expressed in parts per million (ppm), taking tetramethylsilane (TMS) as internal reference. The resulting ^{1}H-NMR data appear coherent with the iodine-grafted cholecalciferol structure by revealing another two new signals that correspond to the two CH aromatic groups at 8.21 and 7.58 ppm of benzene ring (see Supplementary information).

Cholecalciferoyl 2,3,5-triiodobenzoate: ^{1}H NMR ($CDCl_3$, δ/ppm): 8.21 (s, 1H, H^6), 7.58 (s, 1H, H^4), 6.18 (dd, 1H, H^{16}), 5.95 (dd, 1H, H^{15}), 5.15 (m, 1H, H^8), 4.80, 5.08 (s, 2H, H^{12}), 2.76 (t, 2H, H^{18}), 2.64 (t, 2H, H^{13}), 2.43 (d, 2H, H^9), 2.22 (t, 1H, H^{22}), 1.86 (q, 2H, H^{14}), 1.62–1.29 (m, 9H, H^{19}, H^{20}, H^{23}, H^{24}, H^{31}), 1.26 (m, 1H, H^{26}), 1.06 (m, 6H, H^{28}, H^{29}, H^{30}), 0.86 (q, 1H, H^{25}), 0.85 (d, 3H, H^{27}), 0.80 (d, 6H, H^{32}, H^{33}), and 0.47 (s, 3H, H^{34}).

Formulation of Triiodinated Cholecalciferol Nano-Emulsions

Iodinated cholecalciferol nanoparticle emulsions were formulated using a modified method based on spontaneous nano-emulsification as previously described (29,30). Briefly, the principle, illustrated in Fig. 1 (bottom), consisted in mixing the oil phase with non-ionic surfactant and heating this mixture to ensure its homogenization. Then, this phase was

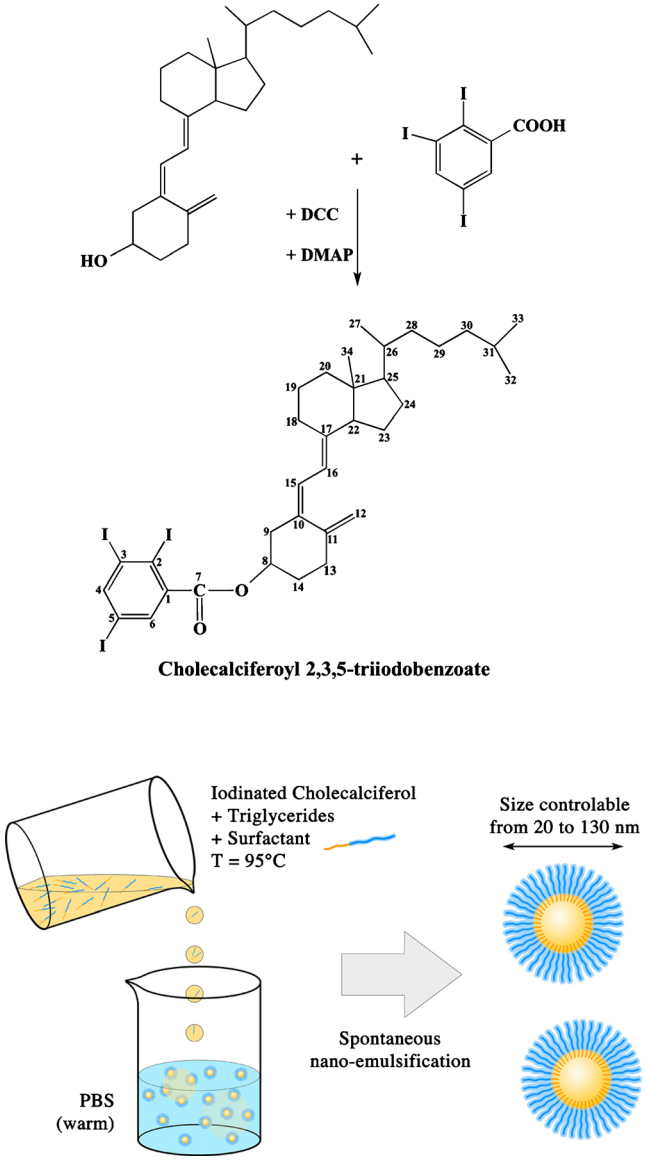

Fig. 1 Synthesis of cholecalciferoyl 2,3,5-triiodobenzoate (*top*). Schematic illustration of the nano-emulsions formulation (*bottom*).

suddenly mixed with warm water, generating the stable nano-emulsions within seconds. In the case of iodinated cholecalciferol, the protocol had been adapted due to the crystalline nature of this compound. Iodinated cholecalciferol was solubilized in another oil (medium chain triglyceride, Labrafac® WL), and this mixture then was added to the non-ionic surfactant.

The nano-emulsion properties, size and size distribution were investigated in function of the formulation parameters: *(i) iodinated cholecalciferol / (iodinated cholecalciferol + triglyceride)* weight ratio (oil ratio, OR), *(ii) surfactant / (surfactant + oil)* weight ratio (SOR) and *(iii) (surfactant + oil) / (surfactant + oil + water)* weight ratio (SOWR). The two representative formulations exhibiting different sizes can be described as follows. The first one, NE_1, is formulated with SOR = 40 wt.%, SOWR = 40 wt.% and OR = 66 wt.%. Triiodinated cholecalciferol (0.065 g) was firstly mixed with triglycerides (Labrafac® WL) (0.033 g), maintained at 95°C with vortex mixing followed by sonication until clear and homogenized solution was obtained. Then nonionic hydrophilic surfactant (Kolliphor ELP®) (0.065 g) was added to the previous solution, and maintained under gentle magnetic stirring alternatively with heating periodically several times. Finally, warm PBS (0.244 g) as an aqueous phase was then poured into the hot solution followed by vortex for 5 min giving rise to formation of the desired nano-emulsion with the average size of 55 nm. The second representative example, NE_2, briefly, is prepared following the same protocol with SOR = 27 wt.%, SOWR = 40 wt.% and OR = 66 wt.% (iodinated cholecalciferol: 0.0986 g, Labrafac® WL: 0.0493 g, Kolliphor ELP®: 0.055 g, PBS: 0.304 g) to give rise to the average diameter around 100 nm. In addition, owing to the fact that the nano-emulsion size is controlled by the surfactant to oil ratio, a slight excess of PBS (0.130 g) and Kolliphor ELP® (0.046 g) were added, in order to provide exactly the same concentrations in all species like for NE_1. In both cases, the value of the SOWR was kept constant at 40% throughout this study, since its influence on the nano-emulsion formation was negligible (it only influenced the droplet concentration) (31). In addition, pH and osmolality of the suspension emulsions were measured and strictly adjusted to obtain a compatibility with parenteral administration. All formulations were repeated three times. Finally, all samples were sterilized by filtration through a 0.22 μm PVDF membrane.

Characterization of Nano-Emulsions by Dynamic Light Scattering (DLS)

The hydrodynamic sizes and polydispersity indices (PDI) of the particles were measured using a dynamic light scattering (DLS) device from Malvern Instruments (Malvern, Orsay, 752 France). The helium/neon laser, 4 mW, was operated at 633 nm with the scatter angle fixed at 173° and the temperature maintained at 25°C. The sizes of the nano-emulsions were determined directly after their formulation. Three different dilutions were prepared 1/1000, 10/1000, and 100/1000 before the measurement. All experiments were performed in triplicate.

In Vitro Studies

Cell Culture. Two different cell lines, namely BNL-CL2 murine hepatocytes and RAW264.7 murine macrophages were grown as monolayer cultures in DMEM medium supplemented with 10% fetal bovine serum (FBS), 100 Unit Penicillin / mL, 100 μg Streptomycin /mL and 2 mM l-glutamine. The culture was maintained in a humidified atmosphere with 5% CO_2.

Stability of Nano-Emulsion Droplets in Serum. Longitudinal size measurements were performed in serum, in order to investigate a potential degradation of the nano-emulsion droplets that may lead to increase or decrease of the droplet size, and potentially influence the pharmacokinetics. Nano-emulsions were incubated in serum for different periods of time.

In Vitro Cytotoxicity (MTT-Assay). The cytotoxicity of the iodinated cholecalciferol nano-emulsion was examined by MTT-test, which has been carried out for two cell lines (BNL-CL2 and RAW264.7 cells). The cells were seeded in 96-well plates (10^4 cells per well) in 100 µL of DMEM and then incubated overnight at 37°C under a controlled atmosphere (5% CO_2 and 80% H_2O). Dilutions of nano-emulsions were made with sterile DMEM to get required concentrations, and then sterilized using 0.22 µm filter. Next, the cell culture medium was replaced by the same medium containing variable concentrations of iodine encapsulated nano-emulsions (corresponding to 0.93, 0.28, 0.093, 0.028, 0.0093, 0.0028, 0.00093, 0.00028 mg I/10^4 cells). After 24 h incubation, the medium was removed and the cells were washed with PBS. Then, the wells were filled with 100 µL of cell culture medium containing MTT (0.5 mg/ml) and incubated for 4 h at 37°C. The obtained formazan crystals were dissolved by adding 100 µL DMSO and the UV absorbance was measured at 570 nm with a microplate reader (Varioskan Flash, Thermo Scientific, USA). Experiments were carried out in triplicate and expressed as a percentage of viable cells compared to the control group.

Cellular Uptake Experiment. *Confocal Microscopy*. The cellular uptake and intracellular localization were determined in RAW264.7 cells (mouse macrophages) and BNL-CL2 (hepatocytes), using a Leica TCS SP confocal scanning system (Leica, Germany). To follow the nano-emulsion droplets, we used a modified lipophilic Nile Red dye (NR668) that was solubilized (0.1 wt.%) in the iodinated oil before formulating the nano-emulsions. NR668 synthesis was previously reported (32). The cells were cultured overnight in cell culture glass chamber slides (5×10^4 cells per well) before their exposition to the dye-loaded nano-emulsions in DMEM supplemented with 10% FBS at a concentration corresponding to 0.1 mg/mL, in a 5% CO_2 humidified atmosphere at 37°C for 30 min, 2 h, and 24 h. After incubation, the cells were stained with Calcein AM (10 µM, 15 min of incubation in Hank's balanced salt solution, HBSS) and with Hoechst 33342 (50 µM, 10 min of incubation in HBSS). After washing for 6 times in HBBS, in order to remove all non-penetrated nano-emulsion droplets, the cells were mounted in the fluorophore protector CC/mount and observed with a Leica confocal microscope equipped with an argon/neon laser and a 63× oil immersion objective. The excitation wavelengths used were 360 nm for Hoechst 33342, 488 nm for Calcein AM, 543 nm for NR668 and the fluorescence signals were collected in the 380–460 nm range for Hoechst, 500–530 nm range for Calcein AM, and 560–650 nm range for Nile Red 668. The images were processed with Fiji software.

Quantification of macrophage uptake. Cellular uptake was quantified by fluorescence spectroscopy. Mouse macrophage RAW264.7 and hepatocyte BNL-CL2 cells were cultured as described above, except that the cells were lysed with DMSO and not mounted for microscopy analysis. The efficacy of washing and lysing was checked with fluorescence microscopy observations. The concentration of the encapsulated NR668 dye in the cell lysate was quantified by fluorimetry with an excitation wavelength of 550 nm and an emission wavelength of 630 nm (with a microplate reader Varioskan Flash, Thermo Scientific, USA). Uptake was expressed as the percentage of fluorescence associated with the cells *versus* the fluorescence in a feed solution.

Micro-CT Imaging

The experiments were performed in agreement with the Committee of Animal Research and Ethics of the University of Lyon-1.

In Vitro Experiments. The X-ray attenuation properties of the iodinated nano-emulsions were evaluated at various concentrations with a micro-CT scanner (1076 Skyscan, Kartuizersweg, Belgium). Experimental parameters were as follows: X-ray, 49 keV, 129 µA; resolution, 35 mm; pitch, 0.4°; aluminum filters, 0.5 and 632 ms. Iodine concentration of nano-emulsions was determined using a calibration curve established with a commercial hydrophilic contrast agent (XenetiX 300, namely iobitridol), correlating iodine concentration and radiopacity.

In Vivo Experiments. *In vivo* imaging experiments were performed with a micro-CT scanner (INVEON, Siemens, Munich, Germany). The experimental X-ray parameters were as follows: X-ray, 50 keV, 500 µA; resolution, 111.25 µm; pitch, 2°; aluminum filters, 0.5 and 900 ms. The acquisitions were performed on Swiss mice, $n=3$, for each type of nano-emulsion. Before the acquisition, mice were anesthetized with isoflurane. Then, the iodinated nano-emulsions were injected using a catheter in the tail vein, with an injection volume corresponding to 10% of the blood volume (i.e., 7.6 µL of nano-emulsions per g of mouse weight). Scans were performed before administration, immediately after injection, and after 30 min, 1, 2, 3, 4, 6 h; 1, 2, 3, 7, 14, 21, 28 and 50 days. The micro-CT raw data were treated with OsiriX viewer to establish 2D maximum projection slices and 3D volume rendering images, and then to quantify a signal by placing a region of interest in the heart, liver, spleen, and kidney.

RESULTS AND DISCUSSION

Spontaneous emulsification is an efficient method for generating stable aqueous suspension of oil nano-droplets. The efficiency of the process is closely dependent on the oil nature, surfactants and their own interactions, solubility in each other (31). When with classical surfactant / oil couples like non-ionic surfactant (Kolliphor ELP®) / triglycerides (Labrafac® WL) the emulsification is very efficient and allows to easily get small stable droplets, this becomes more challenging with more exotic molecules like tri-iodinated cholecalciferol. We have previously reported (11) that in the case of iodinated castor oil, or iodinated monoglycerides, grafting of the triiodobenzoic group affects the process efficiency and leads to the size increase. This phenomenon is likely due to changes in surfactant / oil interactions that may decrease with the tri-iodination. Here, we also observed a change in the emulsification efficiency before and after tri-iodination, namely an enhancement of the efficiency after tri-iodination. Figure 2 shows the effect of the surfactant amount (SOR) for different oil ratios (OR). The values of OR represent the relative percent of cholecalciferol (Fig. 2a) or tri-iodinated cholecalciferol (Fig. 2b) in the oil phase while OR = 0% means that oil phase is pure triglycerides. The corresponding polydispersity indexes are reported in Table S1 (see Supplementary information section). These results clearly demonstrate that the droplet size decreased for the tri-iodinated molecules compared to the native ones. As for the non-iodinated molecules in Fig. 2a, the effect of cholecalciferol in the oil phase appears unfavorable for the lower SOR values. Even if droplet sizes decrease slightly between OR = 0% and OR = 50%, it dramatically grows for a further OR increase up to several orders of magnitudes for OR = 75%. On the other hand, the formulations with tri-iodinated cholecalciferol, in Fig. 2b, is clearly better with smaller droplet size and good monodispersity, and actually, three cases for OR = 50, 66 and 75% appear relatively similar compared to the curve without tri-iodinated cholecalciferol (OR = 0%). PDI values (Table S1) are much better in this latter case, corroborating this observation.

It is noteworthy to understand that the formulations are better when increasing the surfactant concentration (through SOR), but it is to the detriment of the oil amount. In the context of the formulation of X-ray contrast agents, our interest lies in increasing the iodine amount in the droplet. It means that the best formulation should be a compromise between quality of the dispersion and iodine concentration. That is to say, the optimized formulation has the lower SOR with the best dispersion, that could be defined, for example in Fig. 2b, with SOR < 40% and OR = 75%. This figure also allows understanding how a fine control of the nano-emulsion size is performed, in function of the formulation parameters. Moreover, the two different sizes chosen for *in vitro* studies and *in vivo* imaging are indicated with arrows in the graph as NE_1 and NE_2 (for 55 and 100 nm, respectively). The corresponding size distributions obtained by DLS are presented in Fig. 3. It should be noted that they are rather well differentiated to consider them as different sized samples.

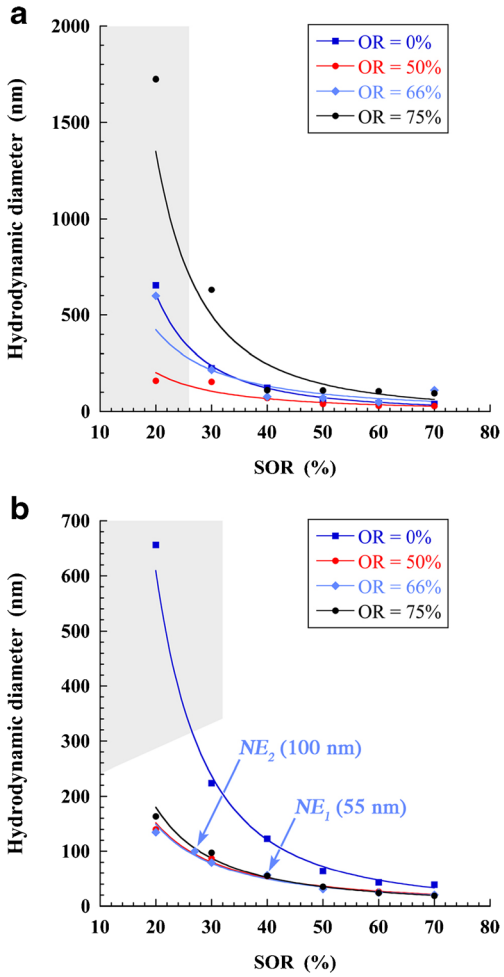

Fig. 2 Effect of the surfactant amount (SOR = surfactant/(surfactant + oil) weight ratio) on the size of the dispersion, function of the relative proportions of cholecalciferol (**a**) and tri-iodinated cholecalciferol (**b**). *Grey* parts indicate globally the regions where nano-emulsions do not form (either size or PDI are too high). NE_1 and NE_2 correspond to the formulations selected for the *in vitro* and *in vivo* studies.

In the following we will focus on the *in vitro* evaluations of these samples, divided in two steps: *(i)* toxicity and stability in the serum, and *(ii)* cell uptake, visualization and quantification. First results have been obtained from viability studies. For this purpose, MTT-tests were performed for two cell lines, in particular macrophages and hepatocytes, and comparing as well NE_1 and NE_2. Results are reported in Fig. 4, and show a clear increase in the toxicity for the bigger nano-emulsions NE_2 compared to NE_1. Even if the toxicity is more marked with macrophages, this trend is conserved whatever the cell line. In the case of macrophages, LD_{50} increases of ΔLD_{50} = 0.35 mg I/mL (from LD50 = 0.21 to 0.56 mg I/mL for NE_2 to NE_1 respectively), and it appears much important in the case

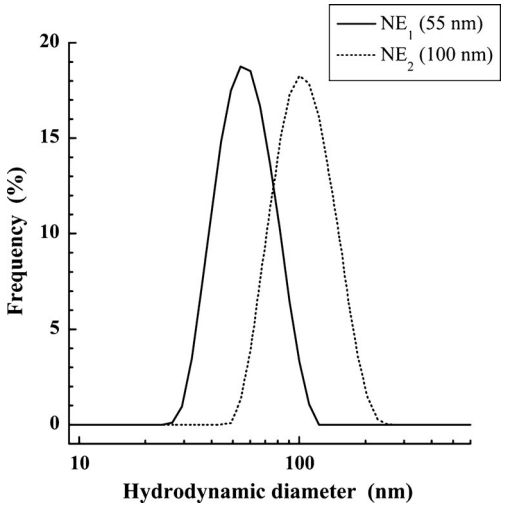

Fig. 3 Size distribution of two nano-emulsions selected for *in vitro* and *in vivo* studies.

of hepatocytes with ΔLD50 = 1.04 mg I/mL (from LD_{50} = 0.75 to 1.79 mg I/mL for NE_2 to NE_1 respectively). These first *in vitro* results disclose a distinct increase of the nano-emulsion toxicity in function of their size: bigger emulsions are slightly more toxic. The second aspect is that macrophages appear more sensitive to the tri-iodinated cholecalciferol than hepatocytes, possibly due to a difference in their interactions with, or uptake of the nano-emulsion droplets compared to hepatocytes.

Another important point to study before performing *in vivo* evaluation is the stability of the suspension in serum. These longitudinal experiments were aimed to simply show physico-chemical stability of the formulation, in order to insure that once injected, the droplets remain stable. As seen in Fig. 5, the relative stability with time whatever the dilutions, which can suggest a compatibility of the stability with the parenteral administration route. This is in the same line with those observed in case of other types of iodinated nano-emulsions (11,33).

Observations of cellular uptake of the iodinated nano-emulsions were performed by confocal microscopy, using a fluorescent probe encapsulated in the oil droplets to reveal their location. The fluorescent dye was a Nile Red lipophilic derivative, namely NR668. This particular dye was chosen owing to the absence of its leakage from the nano-emulsion droplets, ensuring their tracing even in biological media (32). The nano-emulsions were incubated with hepatocytes and macrophages for 30 min and 24 h, then washed and observed. The results are shown in Fig. 6 and disclose that: *(i)* 100 nm droplets are better internalized than 55 nm ones, and *(ii)* the uptake of macrophages was bigger than that of hepatocytes, as expected. For 55 nm droplets, we did not observe any NR688

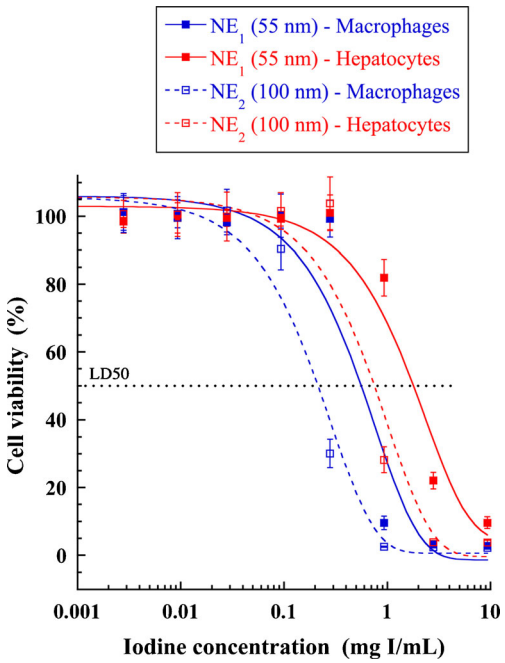

Fig. 4 Viability of the RAW264.7 murine macrophages (*blue* curves) and BNL-CL2 hepatocytes (*red* curves) after 24 h incubation with the iodinated nano-emulsions. The nano-emulsion concentrations were expressed in iodine concentrations per mL. Filled symbols and open symbols correspond to the iodinated nano-emulsions NE_1 and NE_2, respectively.

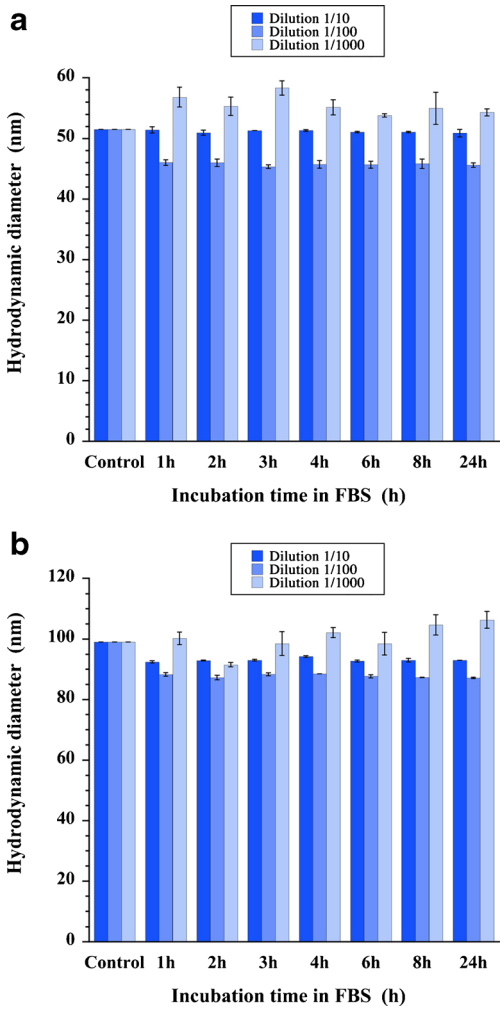

Fig. 5 Stability of nano-emulsions in serum. Average droplet sizes were measured by DLS at different dilutions, for (**a**) NE_1 and (**b**) NE_2.

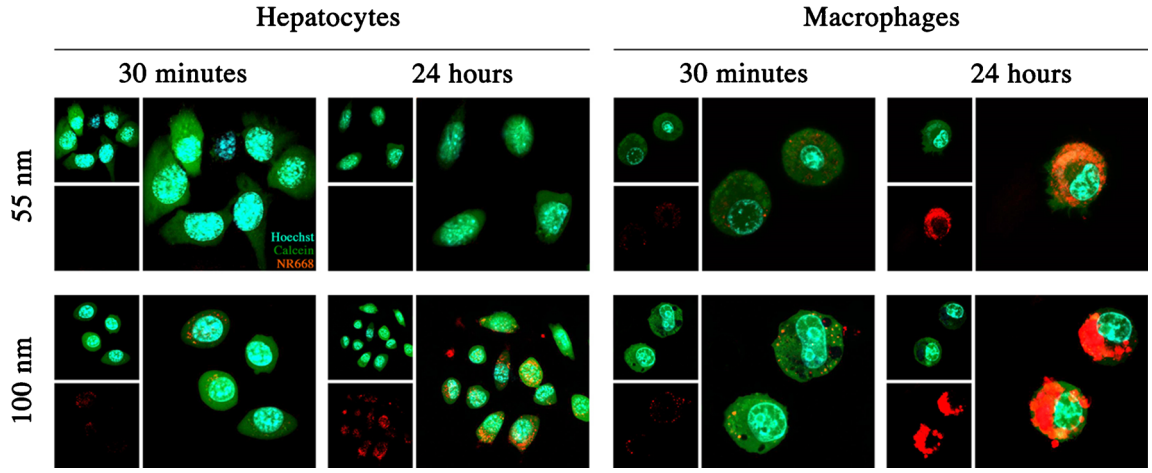

Fig. 6 Monitoring of the uptake of NR668-loaded iodinated nano-emulsions by mouse hepatocytes (BNLCL2) and murine macrophages (RAW264.7 cells) by confocal microscopy. Nuclei were stained with Hoechst (*cyan*) and cells with Calcein AM (*green*). A lipophilic fluorescent dye NR668 was encapsulated in the nano-emulsions, which allowed observing the location of the droplets once engulfed by the cells. The cells were incubated with the nano-emulsions for 30 min and 24 h. *Top left* insets show the cells and nuclei. *Bottom left* insets show the signal and the larger right picture shows both merged.

signal of whatever the incubation time, while for 100 nm ones it was revealed already after 30 min and was clearly visible after 24 h. In the case of macrophages, a similar trend between nano-emulsions of both sizes can be noted but the signal was more pronounced. The quantification of this cell uptake is shown in Fig. 7, which confirmed these observations, and even revealed that after 24 h incubation the quantity of the droplets that were engulfed by the cells doubled in both cases hepatocytes and macrophages. The better accumulation in macrophages of 100 nm PEGylated lipid nano-emulsions compared to the 55 nm one, was demonstrated earlier (34) and could be explained by receptor-mediated phagocytosis (35). Contrary, for the BNL-CL2 cells, which are considered as non-phagocytosis cells, smaller particles are generally better in terms of intracellular accumulation (36). However, the surface properties influence on the uptake significantly: e.g., 100 nm polymeric nanoparticles are able to take up into the non-phagocytic cells more efficiently than those with sizes of 55

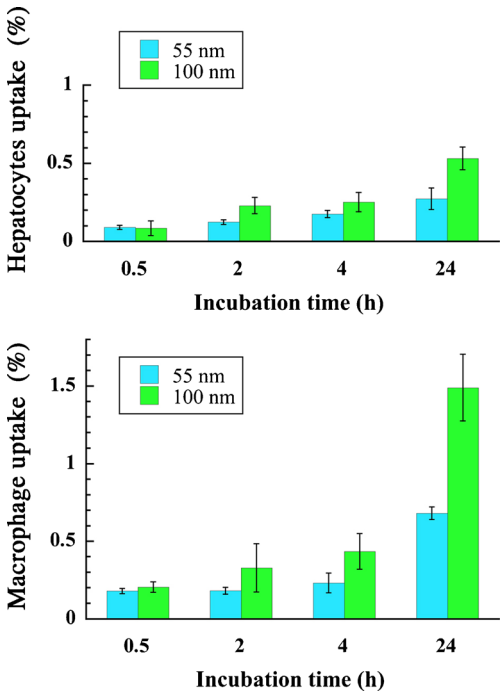

Fig. 7 Quantification of nano-emulsion uptake by hepatocytes and macrophages as a function of the incubation time and droplet size. After incubation with the nano-emulsions loaded with NR668, the hepatocytes or macrophages were washed, lysed with DMSO, and studied by fluorometry. The uptake was expressed as a percentage of fluorescence associated with the cells *versus* fluorescence in a feed solution.

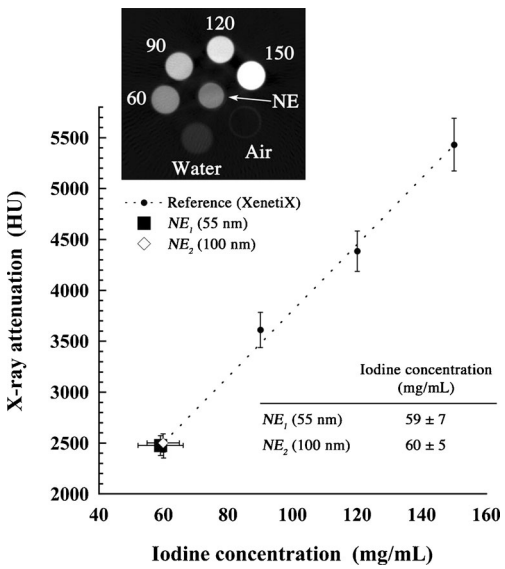

Fig. 8 *In vitro* evaluation of the X-ray attenuation properties of NE_1 and NE_2 using a calibration curve made with iobitridol (filled *circles*). Inset reports the phantom of the tubes (for example one shown for NE_1), with various iodine concentrations as references (expressed in mg/mL), plus water and air for normalization. The table summarizes the values obtained for the nano-emulsions.

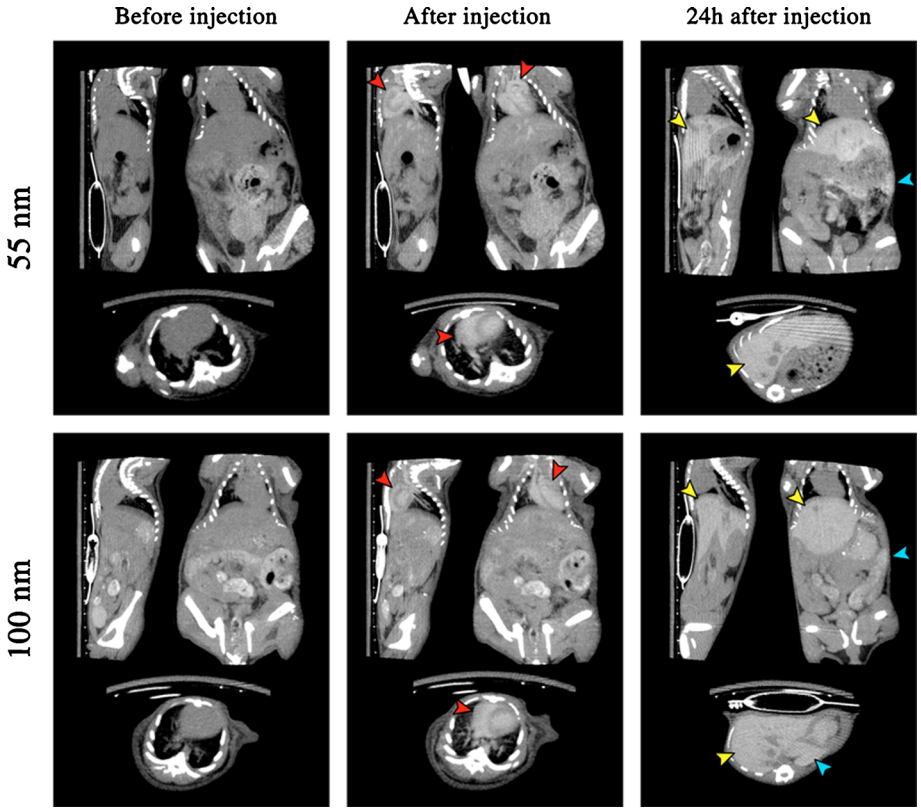

Fig. 9 Left: *in vivo* micro-CT imaging (maximum projection intensity) of the iodinated cholecalciferol nano-emulsions with two different sizes (55 and 100 nm) but with exactly the same composition, before, after and at 24 h after injection (representative times). Pictures show sagittal and coronal sections of the mice, as well as transverse slices through the heart, lung, and vertebra and transverse slices through the liver and spleen. Heart is indicated by red arrowheads, liver by yellow arrows, and spleen by blue arrows. 3D volume rendering is reported as Fig. S1 in *Supplementary Information*, along with two movies corresponding to this volume (movie1.mov and movie2.mov).

or higher than 200 nm (23,37). So the role of surface properties should also be mentioned, however it is not the case in the current study since the surface composition should be similar, only the size effect is studied.

This behavior arises in the same line that the results on cell viability: globally macrophages have a better interactions with the nano-emulsions and they show the highest toxicity, likewise 100 nm droplets also show highest uptake into cells, hepatocytes and macrophages, and also they show the highest toxicity compared to 55 nm ones. All these results corroborate the idea that, the uptake is linked to the toxicity, which should be enhanced with the bigger droplets. Actually, this behavior seems specific to the iodinated cholecalciferol, since with other types of iodinated oils we previously studied like iodinated castor oil or iodinated monoglyceride, droplet internalization were not related to toxicity (uptake were better macrophage and toxicity lower). Eventually, in comparison, iodinated cholecalciferol appears to present a specific toxic activity that can be more pronounced for the bigger droplets.

Let us focus now on the imaging properties and *in vivo* imaging of these contrast agents. The first characterization performed on the samples was the quantification of the iodine content using the X-ray scanner, compared to a commercial hydrophilic contrast agent (XenetiX®). The results, shown in Fig. 8, confirm the similar iodine concentration in both samples, which is around 60 mg/mL and is comparable with the concentrations of the best contrast agents earlier reported (11,33). Based on these *in vitro* observations, we expect a similar contrast in blood pool once injected in mice, which is confirmed visually with the maximum intensity projections in Fig. 9 as well as quantitatively in Fig. 10.

After intravenous administration, we could clearly see the contrast agent spread over the blood compartment emphasizing the heart ventricles main venous and aorta, and even the liver irrigation. After 1 day, the contrast agent was not visible anymore in blood or heart, but has been accumulated in liver and spleen. The 3D volume rendering (see *Supplementary Information*) done on the 55 nm nano-emulsion clearly illustrates the regions containing the contrast agent after injection in blood (red), and in liver at 24 h post-injection (yellow). At first sight, all these images, presented in similar brightness/contrast conditions, seem to show similar properties for the nano-emulsions of two different sizes. However, there is a surprising and heavy difference, which is lethal in case of NE_2 after 48 h post injection. When NE_1 allows a follow-up of the mice during 50 days, NE_2 induces systematically the mice death on the third day post-injection (with $n=6$ in each case). The quantifications of the biodistribution and pharmacokinetics (Fig. 10) show two behaviors almost similar whether it is in blood, liver, spleen or kidney.

First observations, in line with the *in vitro* measurements of X-ray attenuation properties (Fig. 8), confirm the important contrasting properties of this product. The contrast enhancement is significant and allows a clear visualization of the

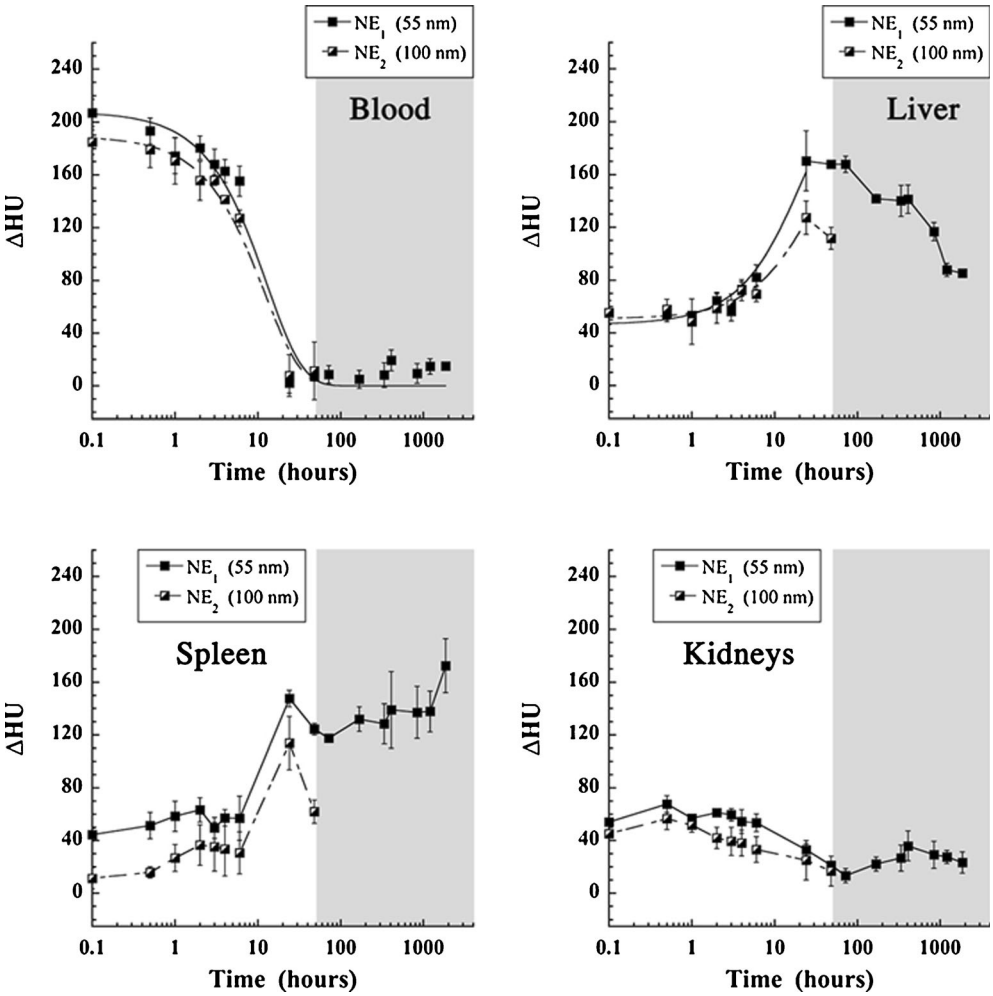

Fig. 10 Quantitative measurements in heart, liver, spleen and kidney of the X-ray attenuation with time after i.v. administration of the iodinated cholecalciferol nano-emulsions. *NE1* and *NE2* refer to the nano-emulsions of the similar composition but different sizes, namely 55 and 100 nm, respectively; $n = 6$ for each nano-emulsion. Curves were fitted with Eq. 1 for the heart (blood elimination) and Eq. 2 for the liver (accumulation). The limit between white and gray part indicates the time for which the mice injected with *NE2* died, whereas the ones injected with *NE1* survived.

regions and tissues where the contrast agent is accumulated, either in blood, liver or spleen. 3D volume rendering gives a more precise idea of the distribution of the contrast agent over the blood compartment, overall, right and left ventricles, liver irrigation, vena cava, hepatic portal vein, and thoracic aorta. One day after injection, arise the location of liver and spleen, indicating that most of the iodinated cholecalciferol has been accumulated in these regions. As for the quantification of the biodistribution of *NE1* and *NE2* over time, the contrast enhancement and kinetics appear almost superimposable for all graphs. In addition, the kinetics of blood clearance and liver accumulation can be fitted with classical mono-compartmental exponential Eqs. (1) and (2), respectively:

$$\Delta\mathrm{HU}(t) = \Delta\mathrm{HU}_0 \times \exp(-k_1.t) \quad (1)$$

$$\Delta\mathrm{HU}(t) = \Delta\mathrm{HU}_0 + \Delta\mathrm{HU}_\infty \times (1 - \exp(-k_2.t)) \quad (2)$$

where $\Delta\mathrm{HU}_0$ is the initial value of the contrast enhancement after injection, $\Delta\mathrm{HU}_\infty$ is the contrast enhancement at the end of the accumulation process, k_1 is the blood elimination rate constant and k_2 is the accumulation rate constant. The obtained pharmacokinetics parameters (reported in Table I) show a close similarity for the blood clearance between both nano-emulsions, with a similar $t_{1/2}$ around 9 h. Moreover, a very similar behavior is observed in the following steps of accumulation / elimination of the contrast agent in liver and spleen up to 24 h post-injection. These observations are confirmed by the similar values of the accumulation rate constant for *NE1* and *NE2*, 0.047 and 0.036 h^{-1}, respectively. However, the values of $\Delta\mathrm{HU}_\infty$ appear a little bit more different, in particular 174 HU and 122 HU, respectively. As

Table I Pharmacokinetics Parameters for the Iodinated Nano-emulsions[a]

	NE1 (55 nm)		*NE2* (100 nm)	
	Blood	Liver	Blood	Liver
$\Delta\mathrm{HU}_0$ (HU)	208	44	189	49
k_1 (h^{-1})	0.077	–	0.081	–
$t_{1/2}$	9.0 h	–	8.5 h	–
k_2 (h^{-1})	–	0.047	–	0.036
$\Delta\mathrm{HU}_{max}$ (HU)	–	90	–	100

[a] $\Delta\mathrm{HU}_{max} = \Delta\mathrm{HU}_0 + \Delta\mathrm{HU}_\infty$

regards the accumulation in spleen, the two curves follow each other up to 24 h, and a dramatic drop of the signal arises at 48 h for NE_2 before the mice death.

It is interesting to compare our product with the main commercial examples like Fenestra® (lipid nano-emulsions), AuroVist® (gold nanoparticle), eXIA 160® (aqueous colloidal iodined dispersion) and ExiTron Nano (rare earth-based nanoparticles) which were studied on the same animal model (mice). In the present contrast agent (iodinated cholecalciferol), the initial contrast enhancement ΔHU = 180–200 HU corresponds to an increase of the contrast of 280–300% (see *Supplementary Information*), which is significantly higher than the 30% of Fenestra® and eXIA 160® in (38), 260% of AuroVist®) in (39) and 240% of ExiTron Nano 12000® in (40). In addition, the half-life of our contrast agent is optimal for CT scans (around 9 h), much longer than eXIA 160® and Fenestra LC® (38), but comparable to the ones reported for Fenestra VC® (38), AuroVist® (39) and ExiTron Nano 12000® (40).

Therefore, we can consider that the size of the nano-emulsions has not a real impact on the whole pharmacokinetics, with a significant difference that arise in the last points before mice death for NE_2, is likely linked to their lethality. On the one hand, we can conclude that the size of the nano-emulsions only slightly affects their fate *in vivo*, but on the other hand, the increase of the size has an irreversible consequence that is the lethal effect on the mice. Actually, the lethality of the iodinated nano-emulsions has never been observed, neither in all the iodinated nano-emulsions we previously synthetized and studied (10,11,33,41,42), nor in literature. This lethality is probably specific and is related to cholecalciferol. Indeed, as seen in Figs. 6 and 7, NE_2 induces cellular uptake which was double higher compared to that in case of NE_1, as well as a higher toxicity (Fig. 4). These two points could orientate the explanation of the size-dependence lethality of the nano-emulsions: although accumulations in liver and spleen appear quite similar in both cases, the total toxicity of NE_2 is probably increased due to a higher cellular uptake. The maximum dosage, which can be supported by the cell, is more rapidly reached with use of the nano-emulsions of the bigger size. This can induce the organ dysfunction and can be considered as an explanation of the loss of the contrast agent concentration before the death, at 48 h.

CONCLUSION

In this study, the question of the influence of the size of the micro-CT nanoparticulate contrast agent on the fate *in vivo* is addressed. The chosen system naturally occurs in living organisms, namely cholecalciferol (or vitamin D_3). We grafted a triiodobenzene motif with radiopaque properties. This new iodinated compound was formulated as nano-emulsions with two different diameters, namely 55 and 100 nm, with exactly the same composition, and then studied *in vitro* and *in vivo* as X-ray contrast agent. The 100 nm nano-emulsions were found to be more toxic than 55 nm ones whatever the cell line (hepatocyte or macrophages). This was likely due to a higher cell uptake, observed by confocal microscopy, and confirmed by fluorimetric quantification. As regard the *in vivo* imaging, the total pharmacokinetics and biodistribution curves in blood, liver, spleen and kidney were quite similar. These results indicate that the nano-emulsion size has no real influence on the *in vivo* fate up to 48 h post-injection. After this time, NE_2 induce the mice death, whereas with NE_1 imaging can be followed up to 50 days without any trouble. This major difference could be attributed to the difference in toxicity and cell uptake related to the droplet size.

ACKNOWLEDGMENTS AND DISCLOSURES

The authors would like to thank for grant "Attractivité IDEX 2013" within University of Strasbourg, France.

REFERENCES

1. Patel HM. Serum opsonins and liposomes: their interaction and opsonophagocytosis. Crit Rev Ther Drug Carrier Syst. 1992;9:39–90.
2. Chonn A, Semple SC, Cullis PR. Association of blood proteins with large unilamellar liposomes in vivo. J Biol Chem. 1992;267:18759–65.
3. Patil S, Gawali S, Patil S, Basu S. Synthesis, characterization and in vitro evaluation of novel vitamin D3 nanoparticles as a versatile platform for drug delivery in cancer therapy. J Mater Chem B. 2013;1:5742–50.
4. Zhang G, Yang Z, Lu W, Zhang R, Huang Q, Tian M, *et al.* Influence of anchoring ligands and particle size on the colloidal stability and in vivo biodistribution of polyethylene glycol-coated gold nanoparticles in tumor-xenografted mice. Biomaterials. 2009;30:1928–36.
5. Aggarwal P, Hall JB, McLeland CB, Dobrovolskaia MA, McNei SE. Nanoparticle interaction with plasma proteins as it relates to particle biodistribution, biocompatibility and therapeutic efficacy. Adv Drug Deliv Rev. 2009;61:428–37.
6. Antonand N, Vandamme TF. Nanotechnology for computed tomography: a real potential recently disclosed. Pharm Res. 2014;31:20–34.
7. Maeda H, Wu J, Sawa T, Matsumura Y, Hori K. Tumor vascular permeability and the EPR effect in macromolecular therapeutics: a review. J Control Release. 2000;65:271–84.
8. Hirsjärvi S, Dufort S, Bastiat G, Saulnier P, Passirani C, Coll J-L, *et al.* Surface modification of lipid nanocapsules with polysaccharides: from physicochemical characteristics to in vivo aspects. Acta Biomater. 2013;9:6686–93.
9. Hallouard F, Anton N, Choquet P, Constantinesco A, Vandamme TF. Iodinated blood pool contrast media for preclinical X-ray imaging applications – a review. Biomaterials. 2010;31:6249–68.
10. Li X, Anton N, Zuber G, Vandamme TF. Contrast agents for preclinical targeted X-ray imaging. Adv Drug Deliv Rev. 2014;76:116–33.

11. Attia MF, Anton N, Chiper M, Akasov R, Anton H, Messaddeq N, *et al.* Biodistribution of X-ray iodinated contrast agent in nano-emulsions is controlled by the chemical nature of the oily core. ACS Nano. 2014;8:10537–50.
12. Holick MF, Tian XQ, Allen M. Evolutionary importance for the membrane enhancement of the production of vitamin D3 in the skin of poikilothermic animals. Proc Natl Acad Sci U S A. 1995;92: 3124–6.
13. MacLaughlin JA, Anderson RR, Holick MF. Spectral character of sunlight modulates photosynthesis of previtamin D3 and its photoisomers in human skin. Science. 1982;216:1001–3.
14. Porter CJH, Trevaskis NL, Charman WN. Lipids and lipid-based formulations: optimizing the oral delivery of lipophilic drugs. Nat Rev Drug Discov. 2007;6:231–48.
15. Holickand MF, Garabedian M. Vitamin D: photobiology, metabolism, mechanism of action, and clinical applications. In: Favus MJ, editor. Primer on the metabolic bone diseases and disorders of mineral metabolism. Washington: American Society for Bone and Mineral Research; 2006. p. 129–37.
16. Holick MF. Phylogenetic and evolutionary aspects of vitamin D from phytoplankton to humans. In: Pangand PKT, Schreibman MP, editors. Vertebrate endocrinology: fundamentals and biomedical implications. San Diego: Academic Press, Inc.; 1989.
17. Holick MF. Physiology, molecular biology, and clinical applications. In: Holick MF, editor. Vitamin D and Health: evolution, biologic functions, and recommended dietary intakes for vitamin D. Totowa: Humana Press Inc.; 2009. p. 3–35.
18. Khlebtsovand N, Dykman L. Biodistribution and toxicity of engineered gold nanoparticles: a review of in vitro and in vivo studies. Chem Soc Rev. 2011;40:1647–71.
19. Oberdörster G, Oberdörster E, Oberdörster J. Concepts of nanoparticle dose metric and response metric. Environ Health Perspect. 2007;115:A290–4.
20. Fadeelaand B, Garcia-Bennett AE. Better safe than sorry: understanding the toxicological properties of inorganic nanoparticles manufactured for biomedical applications. Adv Drug Deliv Rev. 2010;62:362–74.
21. Chono S, Tanino T, Seki T, Morimoto K. Uptake characteristics of liposomes by rat alveolar macrophages: influence of particle size and surface mannose modification. J Pharm Pharmacol. 2007;59: 75–80.
22. Osaki F, Kanamori T, Sando S, Sera T, Aoyama Y. A quantum dot conjugated sugar ball and its cellular uptake. On the size effects of endocytosis in the subviral region. J Am Chem Soc. 2004;126: 6520–1.
23. Winand KY, Feng S-S. Effects of particle size and surface coating on cellular uptake of polymeric nanoparticles for oral delivery of anticancer drugs. Biomaterials. 2005;26:2713–22.
24. Foged C, Brodin B, Frokjaera S, Sundbladb A. Particle size and surface charge affect particle uptake by human dendritic cells in an in vitro model. Int J Pharm. 2005;298:315–22.
25. Chithrani BD, Ghazani AA, Chan WCW. Determining the size and shape dependence of gold nanoparticle uptake into mammalian cells. Nano Lett. 2006;6:662–8.
26. Lu F, Wu S-H, Hung Y, Mou C-Y. Size effect on cell uptake in well-suspended. Uniform mesoporous silica nanoparticles. Small. 2009;5:1408–13.
27. Lee K-D, Nir S, Papahadjopoulos D. Quantitative analysis of liposome-cell interactions in vitro: rate constants of binding and endocytosis with suspension and adherent J774 cells and human monocytes. Biochemistry. 1993;32:889–99.
28. Szebeni J, Muggia FM, Alving CR. Complement activation by cremophor EL as a possible contributor to hypersensitivity to paclitaxel: an in vitro study. J Natl Cancer Inst. 1998;90:300–6.
29. Anton N, Benoit J-P, Saulnier P. Design and production of nanoparticles formulated from nano-emulsion templates—a review. J Control Release. 2008;128:185–99.
30. Anton N, Gayet P, Benoit J-P, Saulnier P. Nano-emulsions and nanocapsules by the PIT method: an investigation on the role of the temperature cycling on the emulsion phase inversion. Int J Pharm. 2007;344:44–52.
31. Antonand N, Vandamme TF. The universality of low-energy nano-emulsification. Int J Pharm. 2009;377:142–7.
32. Klymchenko AS, Roger E, Anton N, Anton H, Shulov I, Vermot J, *et al.* Highly lipophilic fluorescent dyes in nano-emulsions: towards bright nonleaking nano-droplets. RSC Adv. 2012;2:11876–86.
33. Li X, Anton N, Zuber G, Zhao M, Messaddeq N, Hallouard F, *et al.* Iodinated α-tocopherol nano-emulsions as non-toxic contrast agents for preclinical X-ray imaging. Biomaterials. 2013;34:481–91.
34. Vonarbourg A, Passirani C, Saulnier P, Simard P, Leroux JC, Benoit JP. Evaluation of pegylated lipid nanocapsules versus complement system activation and macrophage uptake. J Biomed Mater Res A. 2006;78:620–8.
35. Ohand N, Park JH. Endocytosis and exocytosis of nanoparticles in mammalian cells. Int J Nanomedicine. 2014;9:51–3.
36. Shang L, Nienhaus K, Nienhaus GU. Engineered nanoparticles interacting with cells: size matters. J Nanobiotechnol. 2014;12:1–11.
37. Xu A, Yao M, Xu G, Ying J, Ma W, Li B, *et al.* A physical model for the size-dependent cellular uptake of nanoparticles modified with cationic surfactants. Int J Nanomedicine. 2012;7:3547–54.
38. Willekens I, Lahoutte T, Buls N, Vanhove C, Deklerck R, Bossuyt A, *et al.* Time-course of contrast enhancement in spleen and liver with Exia 160, Fenestra LC, and VC. Mol Imaging Biol. 2009;11: 128–35.
39. Nebuloni L, Kuhn GA, Müller R. A comparative analysis of water-soluble and blood-pool contrast agents for in vivo vascular imaging with micro-CT. Acad Radiol. 2013;20:1247–55.
40. Boll H, Nittka S, Doyon F, Neumaier M, Marx A, Kramer M, *et al.* Micro-CT based experimental liver imaging using a nanoparticulate contrast agent: a longitudinal study in mice. PLoS ONE. 2011;6:e25692.
41. Hallouard F, Briançon S, Anton N, Li X, Vandamme TF, Fessi H. Influence of diblock co-polymer PCL-mPEG and of various iodinated oils on the formulation by the emulsion-diffusion process of radiopaque polymeric nanoparticles. J Pharm Sci. 2013;102:4150–8.
42. Hallouard F, Briançon S, Anton N, Li X, Vandamme TF, Fessi H. Iodinated nano-emulsions as contrast agents for preclinical X-ray imaging, impact of the free surfactants on the pharmacokinetics. Eur J Pharm Biopharm. 2013;83:54–62.